REMOTE SENS. ENVIRON. 48:181–190 (1994)

Surface Characteristics for the Alkali Flats and Dunes Regions at White Sands Missile Range, New Mexico

Robert J. Wheeler, Stuart R. LeCroy,* Charles H. Whitlock,† Gerald C. Purgold,† and Jeffery S. Swanson‡*

Two regions at White Sands Missile Range with different surface reflectance characteristics were studied from November 1988 through December 1991. Continuous 6-min measurements of surface albedo on the alkali flats were used to produce a clear-sky surface climatology for the period. Based on the flats measurements, estimates for a dunes albedo were made using calibrated satellite data. In addition to the surface albedo history, sample bidirectional reflectance characteristics in terms of anisotropic factors for the alkali flats region are also presented. Results show that the flats region is non-Lambertian characterized by large anisotropic factors at high solar and viewing zenith angles. The flat's albedo is highly influenced by surface moisture conditions. Reflectance properties of the dunes are complicated by dune shadows, surface irregularities, seasonal vegetative coverage, and soil moisture.

INTRODUCTION

Because of its surface reflectance characteristics and frequency of clear-sky days, the alkali flats and dunes region at White Sands Missile Range (WSMR) is a highly desirable target for satellite calibration experiments. The highly reflective surface and size of this region makes it easily discernable from the surrounding desert from satellite platforms. Studies by Frouin and Gautier (1987) using dunes-based indirect methods produced calibrations for the GOES 5 and 6 Visible Infrared Spin Scan Radiometer (VISSR) and NOAA-7 Advanced Very High Resolution Radiometer (AVHRR) instruments with uncertainties of ±8–13%. Slater et al. (1987), using more direct flats-based, absolute methods, provided periodic absolute calibration of NOAA AVHRR, Landsat Thematic Mapper (TM), and Satellite Pour l'Observation de la Terre (SPOT) multispectral radiometers with uncertainties of less than ±3%. Nianzeng et al. (1991) provided dunes-based calibration of NOAA-11 AVHRR with uncertainties of ±7.5%.

This document provides more detailed information on the characteristics of two calibration target zones at WSMR which are typically used for on-going satellite calibration or relative intensity studies. On 6 November 1988, NASA's Langley Research Center established the Automated Radiometric Data Acquisition System (ARDAS) on the White Sands alkali flats region. The ARDAS measurements have been used to construct a 38-month clear-sky surface climatology from 7 November 1988 through 31 December 1991.

PHYSICAL CHARACTERISTICS OF THE STUDY AREA

White Sands Missile Range, located in the Tularosa Basin of south-central New Mexico, is a high desert environment with an average elevation of 1250 m. It is bordered by three mountain chains; the Sacramento mountains border to the east and north, the San Andreas to the west, and the Organ mountains to the south. Figures 1 and 2 show horizontal and vertical cross sections of the basin.

*Lockheed Engineering and Sciences Company, Hampton, Virginia
†Atmospheric Sciences Division, NASA Langley Research Center, Hampton, Virginia
‡Army Research Laboratory, White Sands Missile Range, New Mexico
Address correspondence to Robert J. Wheeler, Lockheed Engineering and Sciences Co., 144 Research Dr., Hampton, VA 23666.
Received 9 February 1993; revised 13 November 1993.

0034-4257/94/$7.00

655 Avenue of the Americas, New York, NY 10010

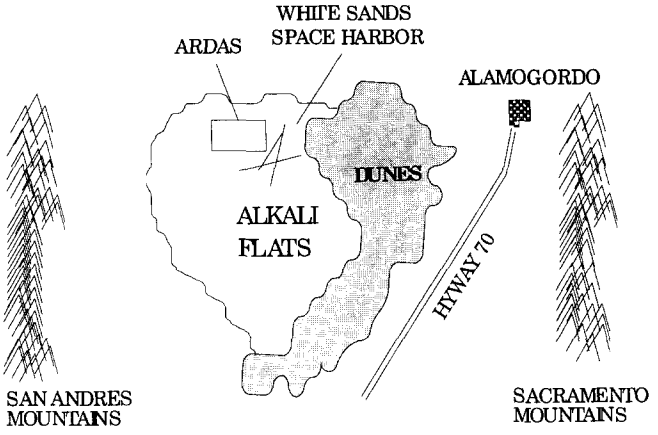

Figure 1. White Sands / Tularosa Basin.

Flats Area

The alkali flats region, located to the west of the dunes, is a wide region of relatively flat, sparsely covered terrain composed primarily of salt compounds, silt, and gypsum (Smith, 1984). Eaton and Dirmhirn (1979) characterized the surface as a crust of algae and lichen stabilized gypsum which becomes darker after a precipitation event. The surface is slightly irregular, made so by both man-made and natural processes.

The surface of the flats is compacted and relatively impermeable to moisture penetration below 5 or 6 cm. For this reason, seasonal lakes form in slight surface depressions during the peak precipitation periods (mid-July to mid-September), though localized seasonal lake formation has been observed following heavy convective precipitation events.

Vegetation on the flats consists primarily of creosote bushes in varying densities. The northern flats region covers about 300 km^2 and has very slight topographic relief. This region was selected for the ARDAS placement because of its relatively large size, uniformity, and lack of significant vegetation. In the ARDAS region, vegetative cover consists of a 1-m diameter creosote bush about every 250 m. Coverage density increases to nearly continuous at the western edge of the flats region and decreases to near zero toward the dunes to the east.

Figure 2. Vertical cross section of Tularosa Basin.

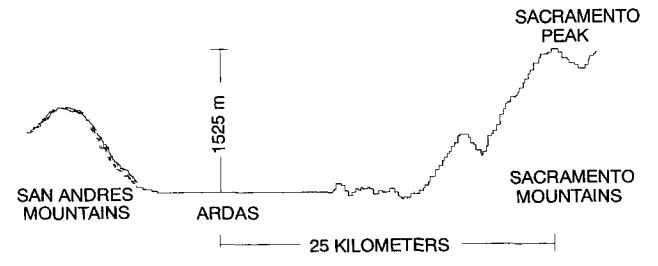

Dunes Region

The dunes region occupies approximately 600 km^2 along the eastern edge of the alkali portion of the basin. This region is highly reflective with albedos approaching 0.85 on the dune crests. The dune surfaces are covered with small ripples approximately 1–2 cm in height, which reduce the surface reflectivity, particularly at high solar zenith angles, by casting small shadows. Figures 3a and 3b show nadir and oblique views of the dunes taken from an altitude of 300 m. These photos were taken in May 1991 at approximately solar noon (solar zenith angle = 20°). Dunes in this region average 6 m from crest to basin. The effect of peak-to-trough shadowing can be seen even at this low solar zenith angle.

Figure 3. Aerial view of dunes region: a) nadir view; b) oblique view.

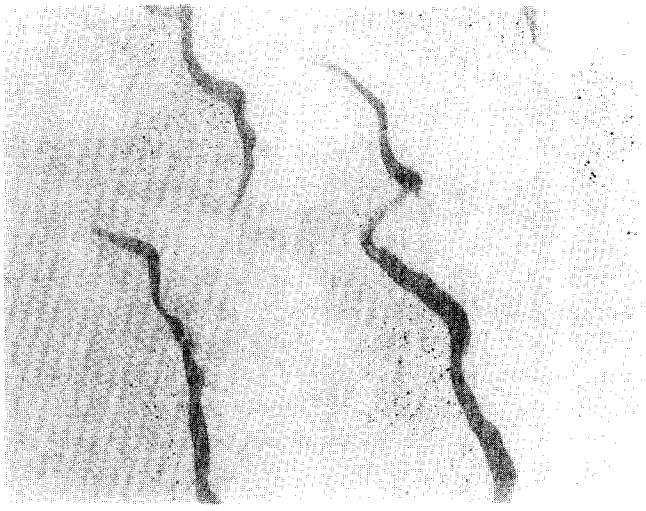

(a)

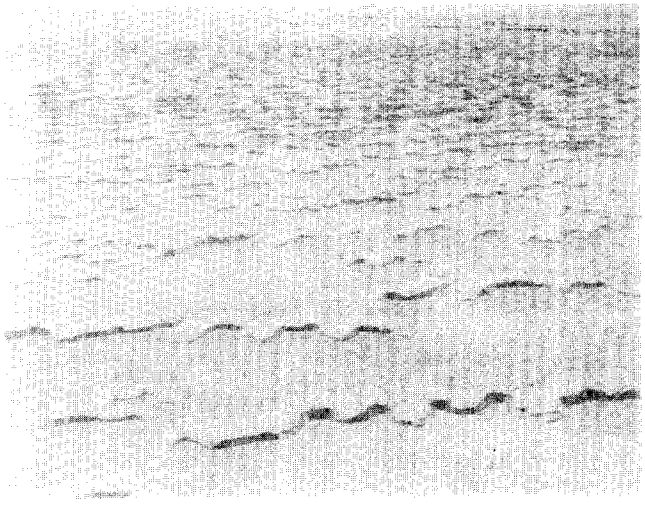

(b)

Diurnal observation of an area large enough to be spatially representative of a 1 km^2 pixel indicates that shadow-induced variation on surface albedo is dynamic with respect to time of day and month of year. Shadow variations complicate the bidirectional reflectance problem and make the dunes a less desirable region for absolute calibration purposes. In addition, the vegetative cover in the low-lying areas between dunes varies seasonally. Vegetation coverage peaks during and directly following the summer monsoonal precipitation period and recedes during the drier months. In a typical year, the dunes region itself moves to the northeast by 4–10 m due to thermal eddy and seasonal wind transport of the gypsum.

During much of the year, thermal eddies pick up substantial quantities of lightweight gypsum dust from the surface of the dunes. The wind-dependent desert aerosol model developed by Longtin et al. (1988) underestimates aerosol loading in the dunes region. In the Longtin desert model, aerosol dust loading does not become significant at wind speeds below 10 m / s. Direct observations of the dunes region suggests that aerosol dust loading of the very fine gypsum dust takes place under conditions at or below 5 m / s.

During May 1991, several daytime observations of the basin region made from Sacramento Peak Solar Observatory showed large diameter, high altitude thermal wind eddies containing the gypsum dust. Figure 4 shows a graphic of the basin from the point of view of an observer during the mid-to-late morning when the surface thermal gradients across the basin were significant. Because gypsum on the flats is stabilized by algae and lichen, eddies cause much less wind-borne dust in that region.

INSTRUMENTATION

The measurement and acquisition network consists of three primary data sites and one ancillary site. The network is located approximately 6 km northwest of the White Sands Space Harbor (WSSH) control tower and 4.5 km northeast of the Drew Site observation mound in the northern flats (Fig. 5). The distribution of sites was selected to approximate the areal coverage of a 1-km satellite pixel. Sites 1 and 3 were instrumented primarily with radiometers while Sites 2 and 4 had both radiometric and meteorological sensors. Site 4 contained redundant downwelling sensors, a site barometer, and

Figure 4. Thermal eddy transport of gypsum dust.

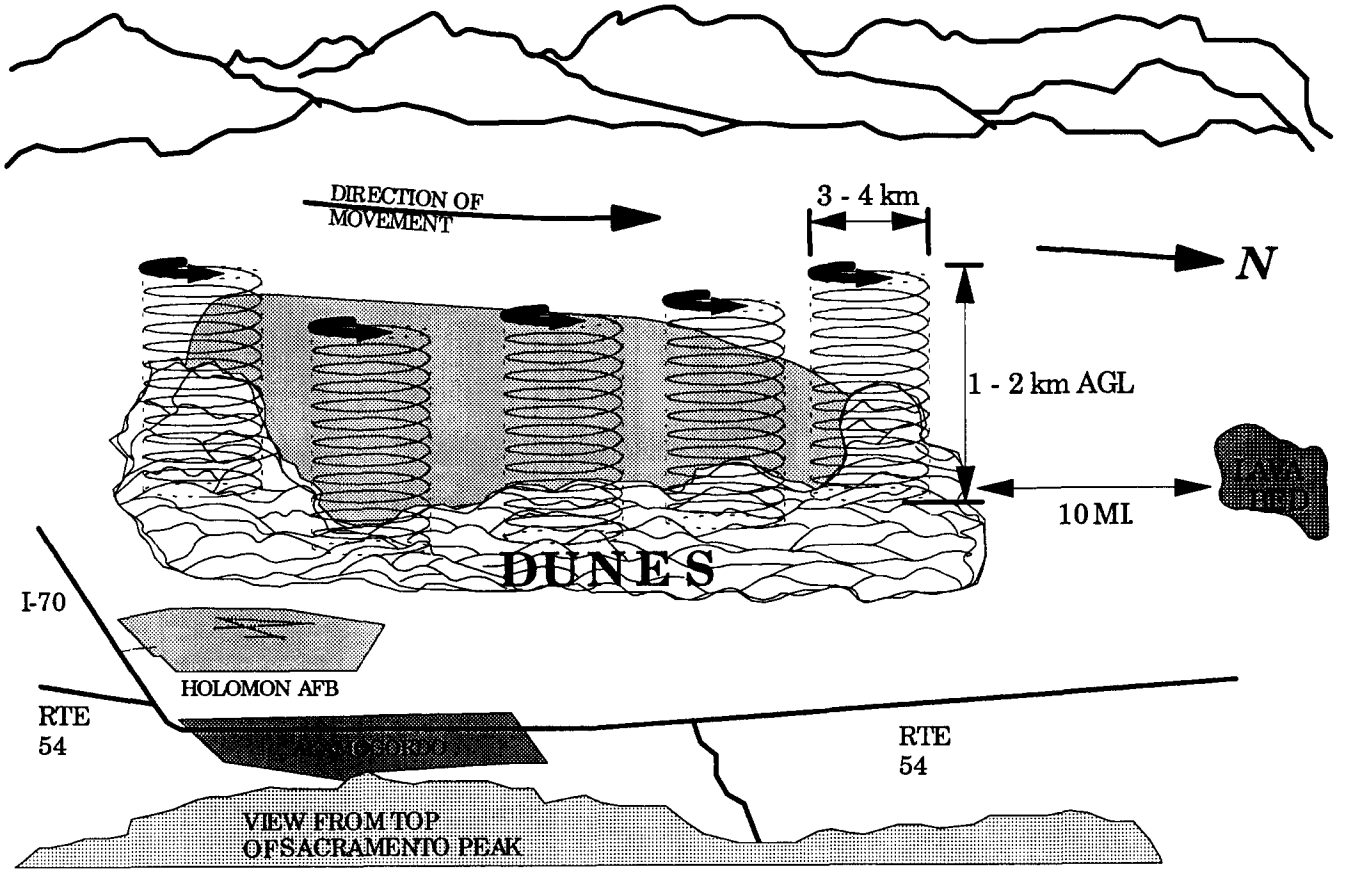

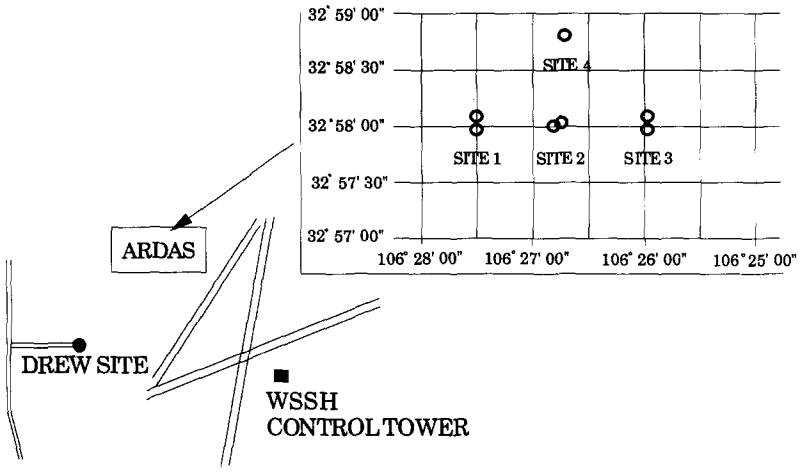

Figure 5. WSMR flats ARDAS site location.

multilevel soil temperature probes. The probes measured soil temperatures at 2 cm and 4 cm below the surface.

Figures 6a and 6b show aerial views of ARDAS Sites 1 and 2, respectively. Pyranometer complements at Sites 1 and 3 consisted of narrowband Licor Industries LI-210 SB pyranometers with a spectral range of 0.5–0.6 μm and medium band Li-200 SB pyranometers with a spectral range of 0.38–1.1 μm. One pyranometer of each type was mounted in a down-looking mode on towers located 50 m north and south of the site center. Each down-looking tower was 6 m in height with a 1-m boom arm assembly which supported the instruments. Another sensor of each type was mounted on a flat plate in an up-looking orientation. Albedo measurements were calculated in a relative manner for each site using the ratio of the average upwelling to the downwelling responses.

The Site 2 sensor complement included temperature/humidity and wind monitor sensors in addition to the Licor Industries LI-200 and 210 pyranometers. Additionally, one set of Eppley PSP broadband radiometers (spectral range = 0.28–2.8 μm) was located at the central site. Broadband albedos were computed in the same relative manner as the other sites, but are representative of a single point location at Site 2.

SPATIAL CORRECTION

In an effort to measure the spatial variability of surface brightness for the ARDAS region under a variety of different moisture conditions, several spatially corrected 20-m-resolution clear-sky SPOT multispectral scenes were selected. These scenes correspond to the widest variation in surface albedos observed during the period from clear-sky scenes.

Using a manual landmark navigation method, the location of the ARDAS down-looking pyranometer

Figure 6. Aerial view of ARDAS sites: a) Site 1 (westernmost); b) Site 2 (central).

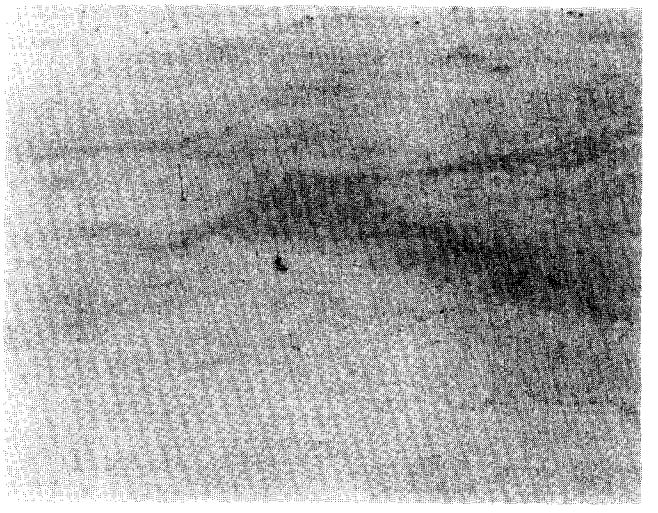

(a)

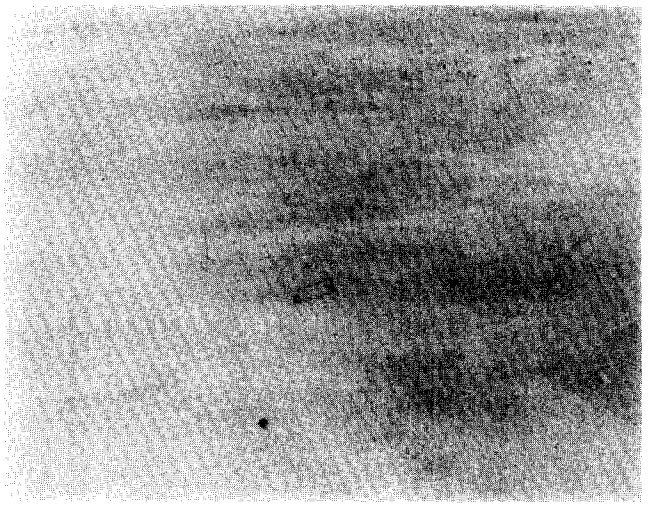

(b)

towers was determined to within one 20-m pixel for the six primary down-looking narrowband instruments for each scene. The pixel counts at these six locations were then averaged to yield a "site-average." Using the location of the Site 2 up-looking instrument platform as the center, box boundaries for 1 km^2, 2 km^2, and 3 km^2 regions were determined. Pixels within these boundaries were then averaged to yield "box" pixel counts. Figure 7 shows the location of these boxes with respect to ARDAS and the White Sands Space Harbor runways. The average box counts were then compared to the site-average pixel counts to determine a site-to-box spatial correction. The expanded 2 km^2 and 3 km^2 regional corrections are necessary to meet calibration requirements for operational weather satellites with variable viewing angles.

SPOT multispectral Bands 2 and 3 cover approximately the same spectral range as the GOES and NOAA AVHRR visible channels. By averaging the 3-km box corrections for these two bands and comparing the results with measured surface albedos for five cases, the spatial correction necessary for any given albedo (see Fig. 8) is

$$C_a = \frac{S_a}{0.12*\ln(S_a) + 1.12}, \quad (1)$$

where

C_a = spatially corrected surface albedo for the 3-km box,
S_a = site-average measured surface albedo.

Figure 7. ARDAS 1-km, 2-km, and 3-km boxes with respect to White Sands Space Harbor runways.

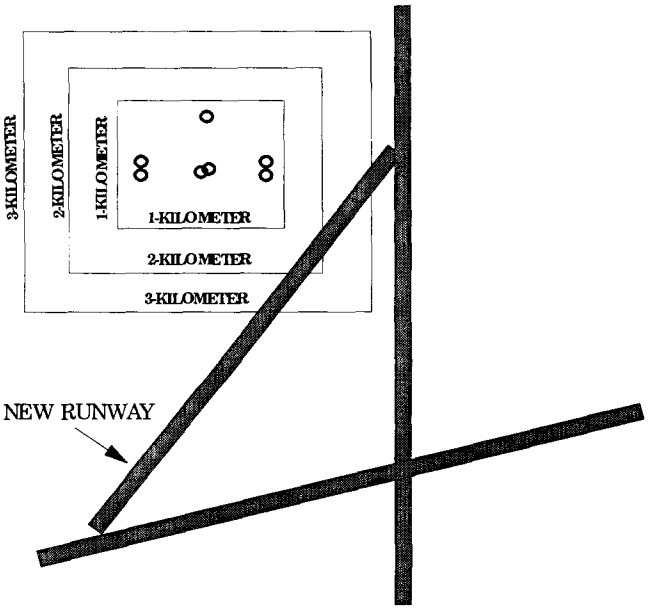

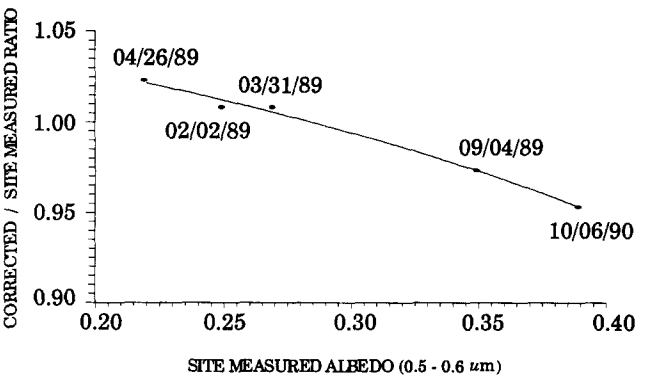

Figure 8. Spatial correction.

CALIBRATION CLEAR-SKY CLIMATOLOGY

Acceptable clear-sky days for satellite calibration purposes were defined using downwelling irradiance to detect clouds and a minimum surface albedo threshold to detect surface standing water. Downwelling irradiance curves could not exhibit abnormal perturbations from clouds or dust for the entire day from sunrise to sunset. Surface albedos less than 0.20 indicate the presence of standing water on the alkali surface. Saturated surface conditions or standing water results in unreliable bidirectional reflectance characteristics; therefore, data meeting this criteria were eliminated from the study. As of 7 November 1991 ARDAS had been operational for 1095 days. There were 241 calibration clear-sky days during this period. Twenty additional days were disregarded due to low surface albedo and the probability of saturated surface conditions. In addition, 18 clear-sky days were sacrificed for pyranometer calibration purposes, leaving a total of 203 acceptable clear-sky days. The monthly distribution of acceptable calibration clear-sky days from 7 November 1988 to 6 November 1991 is shown in Figure 9. Most calibration clear-sky days occurred during the late fall months from

Figure 9. Monthly distribution of clear-sky days 7 November 1988–6 November 1991.

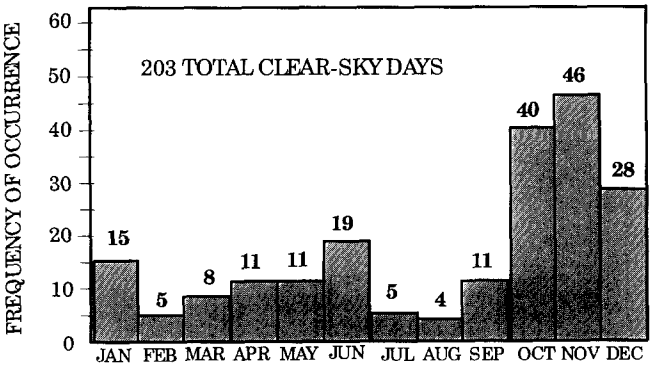

October to December. During this period, an additional 314 additional days met the criteria for marginal clear-sky days (clear ±2 h from solar noon).

CLEAR-SKY SURFACE ALBEDO CHARACTERISTICS

Flats Region

Annual Variability

Moisture appears to have the greatest impact on surface albedo (Smith, 1984). Figure 10 shows solar noon clear-sky narrow-band corrected albedos for each of the three operational measurement years. The trend in these data corresponds inversely to the observed annual precipitation trend; the lowest albedos correspond to periods in which precipitation events are more prevalent. Highest albedos occur during November to January when precipitation events are few and generally light. Due to the relative impermeability of the flats surface, water saturation occurs rapidly. Only a small portion of the surface moisture following a precipitation event percolates into the surface, but rather runs off and pools in depressions and then dissipates through evaporation. This albedo recovery or "drying out" period is generally short through most of the annual cycle with albedos generally rising rapidly over the span of a few days. However, during the monsoonal precipitation months in the summer, repeated precipitation events result in lower surface albedos for extended periods. During these periods algae blooms darken the surface considerably, giving it a mottled appearance and suppressing albedos until the surface dries substantially and the algae recedes.

Diurnal Variability

As in the case of annual variability, moisture has the greatest impact on diurnal albedo variability. Daily 6-min albedo curves for the flats region show the effect of surface moisture on albedo during several daily cycles (Fig. 11). On 25 January 1991, dew formed on the surface during the overnight hours. The dew evaporated during the mid-to-late morning hours increasing the surface albedo by nearly 30%. The 17 March 1991 curve shows a similar trend, though the surface dew evaporated more quickly in the presence of higher surface wind speeds and higher temperatures.

Conversely, the data for 3 June 1991 show a fairly flat response with less than 3% variation throughout the day. This relative stability is the result of a fairly uniform moist surface under algae bloom conditions, low winds, and high relative humidities. The curve for 10 April 1991 has similar characteristics, though the surface is much drier as indicated by the higher albedos.

Dunes Region

Annual Variability

A dunes region measuring 7 km east to west and 6 km north to south was determined using several SPOT 20-m resolution multispectral scenes. The location of this region with respect to the ARDAS network and surrounding features is shown in Figure 12. The region extends south and east from 32° 59′ north and 106° 22′ 30″ west. Nianzeng (personal communication, 1992) identified the central portion of this region as possessing a high degree of reflective homogeneity, making it a more desirable dunes location from which to perform calibrations. Direct examination of the region shows relatively uniform dune orientation consistent with dune region movement to the northeast and extremely sparse vegetation content.

Dunes albedo measurements are derived from ARDAS-calibrated GOES-7 visible channel radiances and spatially corrected narrowband alkali flats albedos. The ARDAS region GOES-7 visible radiances were computed using an average count for the 3 km × 3 km region

Figure 10. Solar noon clear-sky narrowband albedos.

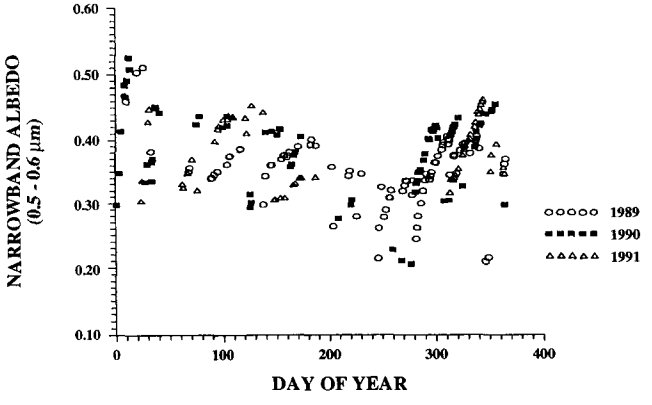

Figure 11. Narrowband diurnal albedos for selected cases.

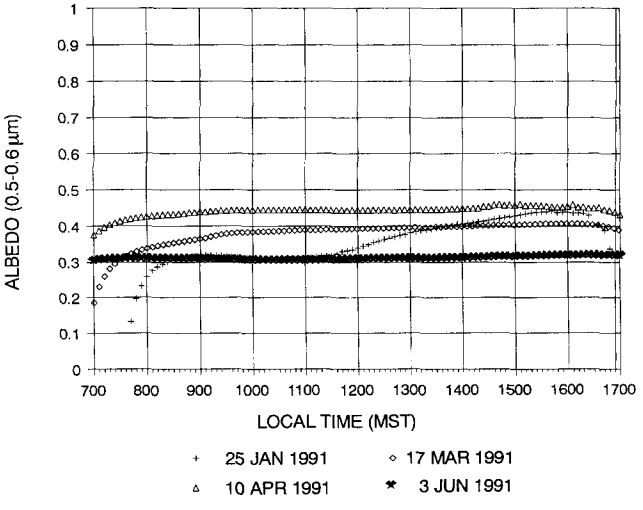

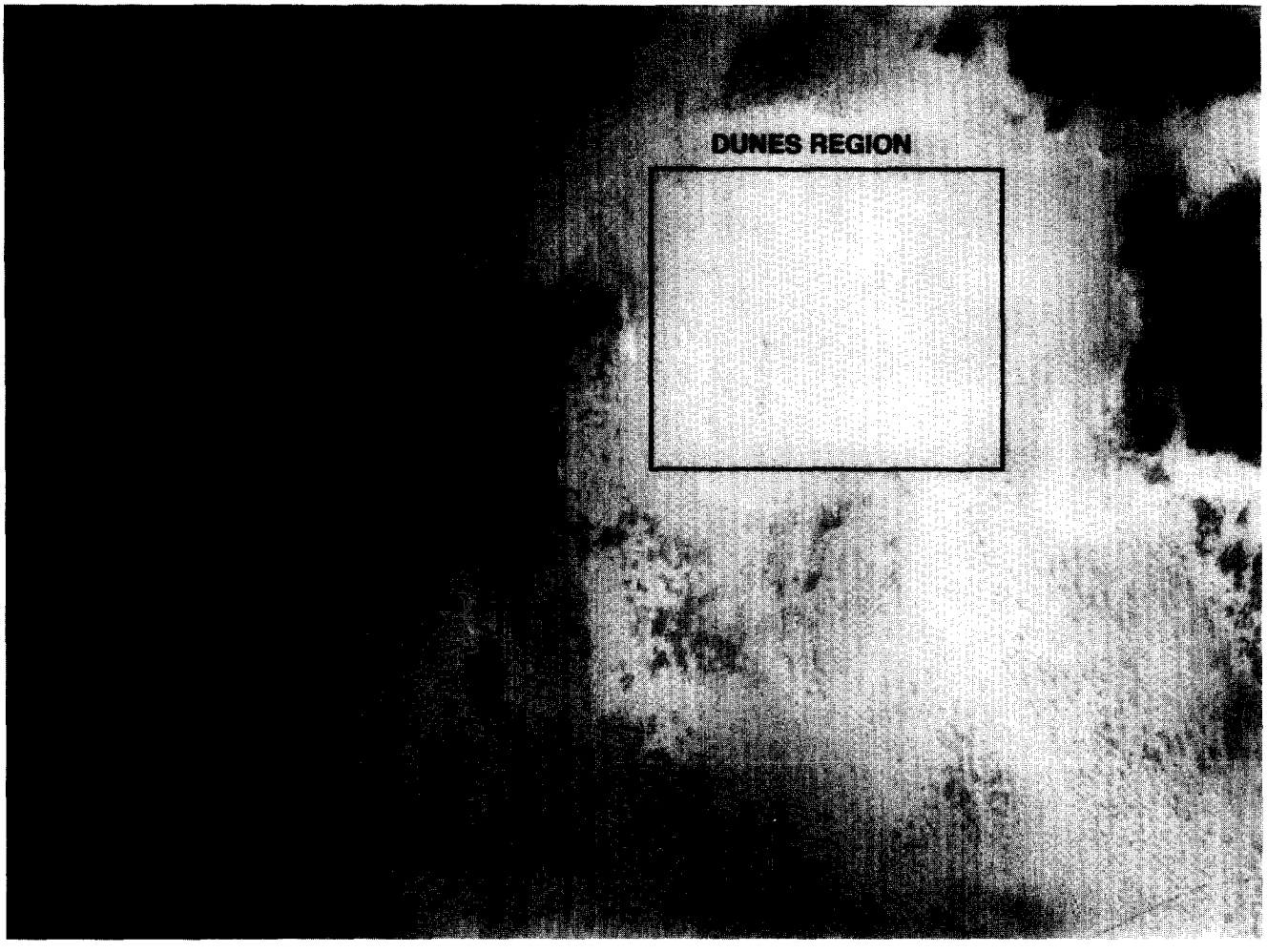

Figure 12. ARDAS flats and dunes regions.

previously defined in Figure 6. Radiances for the flats and dunes subregions were computed using

$$L = \frac{1}{G} * C^2 - 1, \qquad (2)$$

where

L = GOES 7 visible radiance (W / m^2 μm sr),
G = gain,
C = GOES 7 8-bit counts.

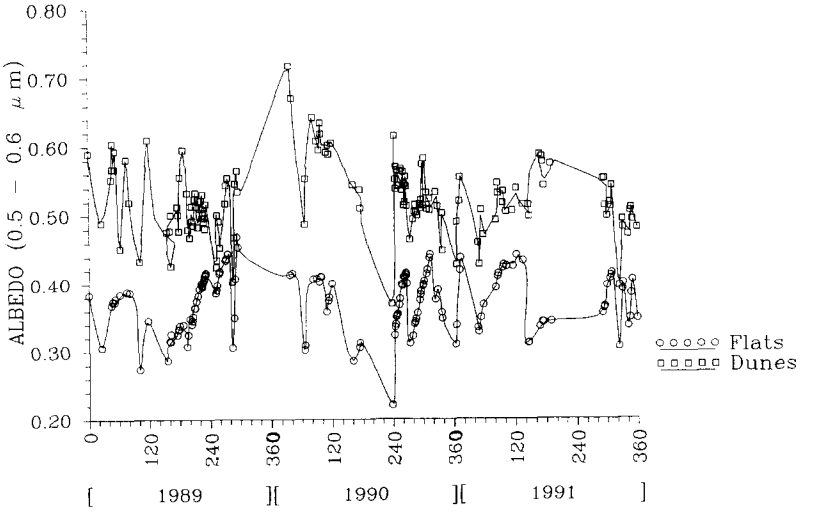

Figure 13. Flats measured versus dunes computed narrowband clear-sky solar noon albedos.

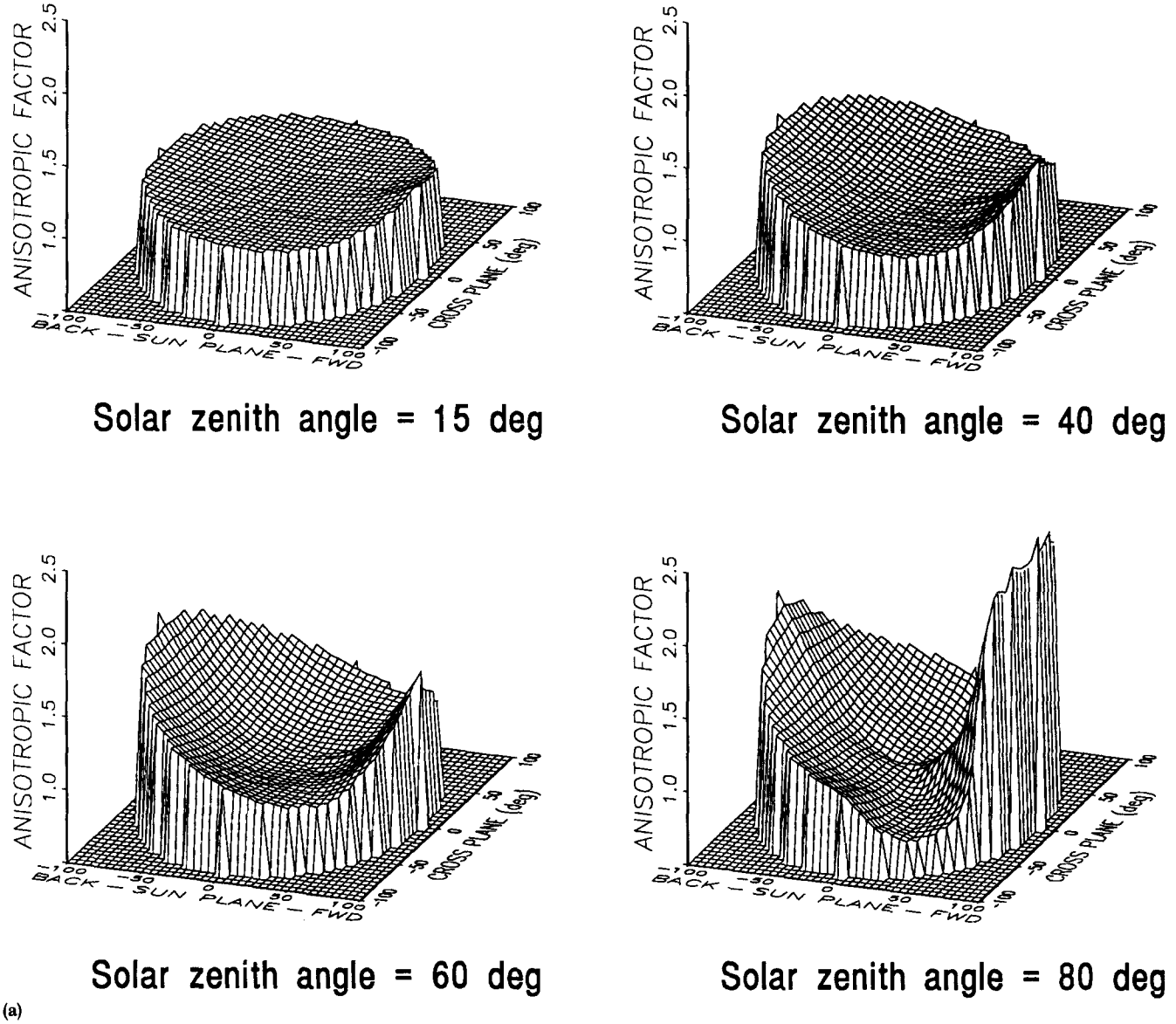

(a)

Figure 14a. Anisotropic factors for moist surface (albedo = 0.30).

The dunes narrowband albedo was then estimated using the clear sky narrowband albedo and radiances for each site as follows:

$$A_d = \frac{L_d}{L_f} * A_f \qquad (3)$$

where

A_d = dunes shortwave albedo,
L_d = dunes visible radiance,
L_f = flats visible radiance,
A_f = flats shortwave albedo.

Figure 13 shows flats and dunes calibration clear-sky albedos for the measurement period. Both regions experience large variations in albedo magnitude. The numerous short-term divergences between flats and dunes traces are thought to be the result of localized precipitation events occurring primarily over one region but not the other or the effects of dunes shadowing on a seasonal basis.

ANISOTROPIC CHARACTERISTICS FOR THE FLATS REGION

Bidirectional reflectance measurements were conducted at the ARDAS site using a four-channel radiometer mounted on-board a helicopter (Purgold et al., 1993). Detailed measurements in zenith and azimuth were obtained to determine the bidirectional characteristics as a function of solar zenith angle. The results were

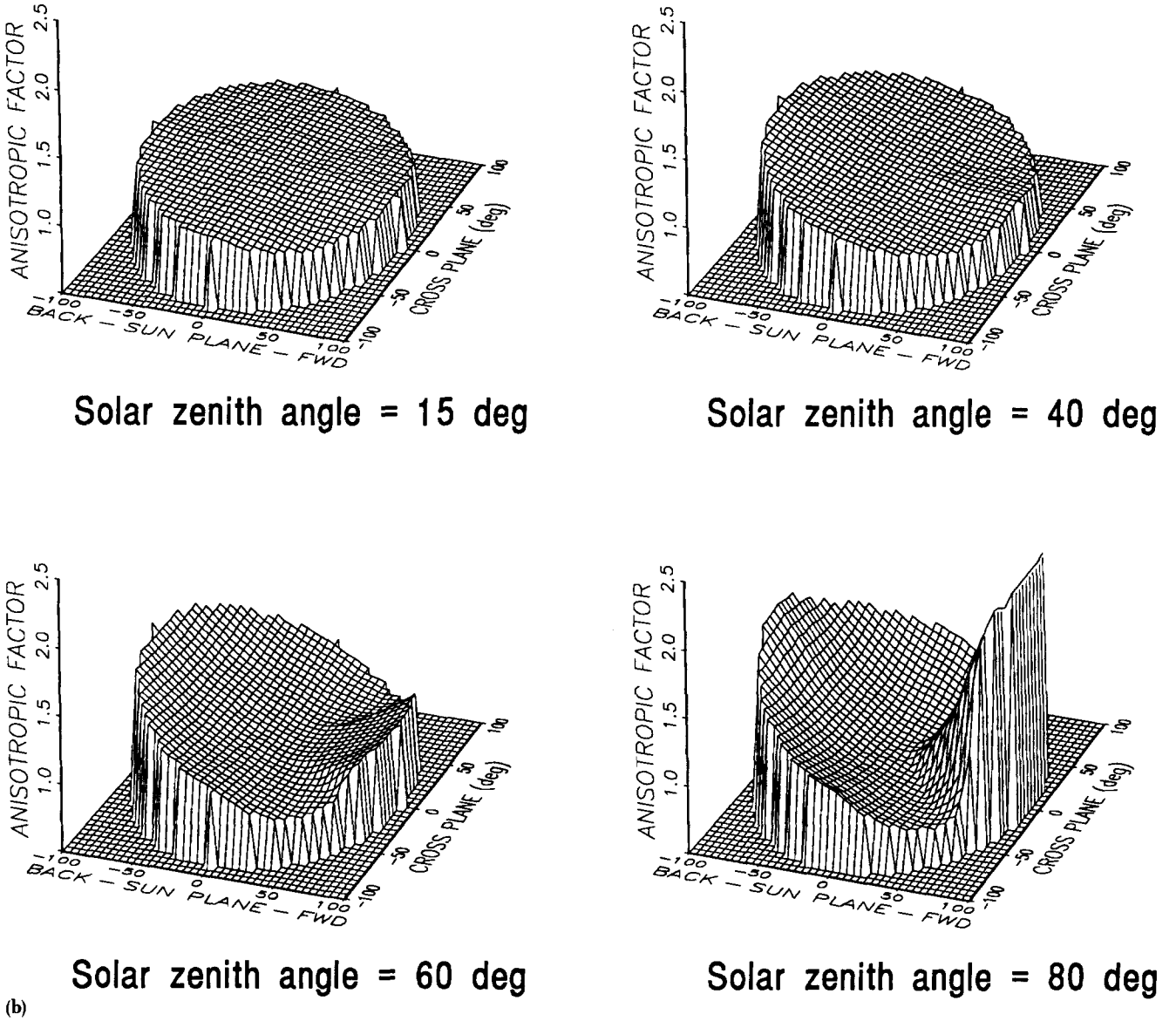

(b)

Figure 14b. Anisotropic factors for dry surface (albedo = 0.42).

converted to an anisotropic function defined by Suttles et al. (1988) as the ratio of the equivalent lambertian flux to the actual flux. Figures 14a and 14b show sample anisotropic factors for marginally moist (albedo = 0.30) and dry (albedo = 0.42) surfaces at 0.65 μm. The measurements show that the flats surface at White Sands is anisotropic particularly at high viewing and solar zenith angles. Complete bidirectional measurement results as a function of wavelength and soil moisture are presented in Whitlock et al. (1993).

CONCLUDING REMARKS

Surface albedo for both the alkali flats and dunes regions is heavily dependent on moisture. There is a strong correlation between month of year and surface brightness.

Flats albedo recovery is relatively quick during the dry season, but can take several days to weeks during peak precipitation periods. The recovery period for the flats is apparently lengthened due to the effect of moist season algae bloom. Diurnal-dew effects are also seasonal. During moist periods, surface albedos tend to remain stable through the course of the diurnal cycle. Conversely, during drier periods, dew evaporation can result in changes in surface albedo by as much as 30% during a normal clear-sky day. The flats region is a non-Lambertian surface characterized by large anisotropic factors at high viewing and solar zenith angles.

The authors are indebted to Dr. Robert A. Schiffer (World Climate Research Programme Radiation Projects Office, NASA Headquarters) and Dr. James C. Dodge (NASA Headquarters) for their guidance and support for this research.

REFERENCES

Eaton, F. D., and Dirmhirn, I. (1979), Reflected irradiance indicatrices of natural surfaces and their effect on albedo, *Appl. Opt.* 18:994–1008.

Frouin, R., and Gautier, C. (1987), Calibration of NOAA-7 AVHRR, GOES-5, and GOES-6 VISSR/VAS solar channels, *Remote Sens. Environ.* 22:73–101.

Longtin, D. R., Shettle, E., Hummel, J., and Pryce, J. (1988), A wind dependent desert aerosol model: radiative properties, Air Force Geophysics Laboratory, Scientific Report No. 6, Monitoring Organization Report No. AFGL-TR-88-0112, Hanscom Air Force Base, Massachusetts.

Nianzeng, C., Grant, B., Flittner, D., Slater, P., and Biggar, S. (1991), Results of calibrations of the NOAA-11 AVHRR made by reference to calibrated SPOT imagery at White Sands, N.M., *SPIE Proc.* 1943:21.

Purgold, G. C., Whitlock, C., Wheeler, R., and LeCroy, S. (1993), A multi-wavelength Airborne Radiometer Scanner (ARS) for measuring surface bidirectional reflectance characteristics, *Remote Sens. Environ.*, forthcoming.

Slater, P. N., Biggar, S. F., Holm, R., et al. (1987), Reflectance and radiance-based methods for the in-flight absolute calibration of multispectral sensors, *Remote Sens. Environ.* 22: 11–37.

Smith, G. R. (1984), Surface soil moisture measurements of the White Sands, New Mexico, NOAA Technical Memorandum NESDIS 7, Washington, D.C.

Suttles, J. T., Green, R. N., Minnis, P., et al. (1988), *Angular Radiation Models for Earth–Atmosphere System, Vol. I—Shortwave Radiation*, NASA RP-1184, Hampton, Virginia.

Whitlock, C. H., LeCroy, S. R., and Wheeler R. J. (1993), Narrowband angular reflectance properties of the alkali flats at White Sands, New Mexico, *Remote Sens. Environ.*, forthcoming.